Neurochemistry International 141 (2020) 104870

Contents lists available at ScienceDirect

Neurochemistry International

journal homepage: www.elsevier.com/locate/neuint

Efficacy and pharmacokinetics evaluation of 4-(2-chloro-4-fluorobenzyl)-3-(2-thienyl)-1,2,4-oxadiazol-5(4H)-one (GM-90432) as an anti-seizure agent

Kyu-Seok Hwang [a,1], Hyemin Kan [a,1], Seong Soon Kim [a], Jin Sil Chae [a], Jung Yoon Yang [a], Dae-Seop Shin [a], Se Hwan Ahn [b], Jin Hee Ahn [b], Jin-Hwa Cho [c], Il-Sung Jang [c,d], Junnyeong Shin [e], Jaeyoung Joo [e,f], Cheol-Hee Kim [g], Myung Ae Bae [a,*]

[a] Drug Discovery Platform Research Center, Korea Research Institute of Chemical Technology, Daejeon, 34114, Republic of Korea
[b] Department of Chemistry, Gwangju Institute of Science and Technology, Gwangju, 61005, Republic of Korea
[c] Department of Pharmacology, School of Dentistry, Kyungpook National University, Daegu, 41940, Republic of Korea
[d] Brain Science and Engineering Institute, Kyungpook National University, Daegu, 41940, Republic of Korea
[e] Zefit. Inc., Daegu, 42988, Republic of Korea
[f] School of Undergraduate Studies, Daegu Gyeongbuk Institute of Science and Technology, Daegu, 41940, Republic of Korea
[g] Department of Biology, Chungnam National University, Daejeon, 34114, Republic of Korea

ARTICLE INFO

Keywords:
Zebrafish
Anti-seizure drug
Electroencephalogram
Electrophysiology
Pharmacokinetics

ABSTRACT

Epilepsy is a common chronic neurological disease characterized by recurrent epileptic seizures. A seizure is an uncontrolled electrical activity in the brain that can cause different levels of behavior, emotion, and consciousness. One-third of patients fail to receive sufficient seizure control, even though more than fifty FDA-approved anti-seizure drugs (ASDs) are available. In this study, we attempted small molecule screening to identify potential therapeutic agents for the treatment of seizures using seizure-induced animal models. Through behavioral phenotype-based screening, 4-(2-chloro-4-fluorobenzyl)-3-(2-thienyl)-1,2,4-oxadiazol-5(4H)-one (GM-90432) was identified as a prototype. GM-90432 treatment effectively decreased seizure-like behaviors in zebrafish and mice with chemically induced seizures. These results were consistent with decreased neuronal activity through immunohistochemistry for pERK in zebrafish larvae. Additionally, electroencephalogram (EEG) analysis revealed that GM-90432 decreases seizure-specific EEG events in adult zebrafish. Moreover, we revealed the preferential binding of GM-90432 to voltage-gated Na^+ channels using a whole-cell patch clamp technique. Through pharmacokinetic analysis, GM-90432 effectively penetrated the blood-brain barrier and was distributed into the brain. Taken together, we suggest that GM-90432 has the potential to be developed into a new ASD candidate.

1. Introduction

Epilepsy is a disorder of the central nervous system (CNS) with repeated excessive neuronal activity in patients, which are known as seizure. It is one of the most common neurological diseases, affecting more than approximately 50 million people worldwide (World Health Organization, 2019). According to the International League Against Epilepsy (ILAE), epilepsy has a multilevel classification in the order of clinical seizure types, epilepsy types, and epilepsy syndromes (Scheffer et al., 2017). A person with two or more unprovoked seizures is considered epileptic (Goldenberg, 2010), therefore, seizures are a basic symptom for diagnosing epilepsy. Despite more than 20 anti-seizure drugs (ASDs) being used in patients, most have been identified as efficacious based on randomized clinical trials or using seizure-induced models (Wilcox et al., 2013). Moreover, at least 25–40% of newly diagnosed epilepsy patients are estimated that continue to have seizures due to drug resistance (Wilcox et al., 2013; Schmidt and Sillanpää, 2012). Therefore, there is a significant need for the development of safer ASDs that are more effective against drug-resistant seizures.

Most ASDs have been developed with the primary goal of stopping

* Corresponding author. Drug Discovery Platform Research Center, Korea Research Institute of Chemical Technology, Daejeon, 34114, Republic of Korea.
E-mail address: mbae@krict.re.kr (M.A. Bae).
[1] Kyu-Seok Hwang and Hyemin Kan contributed equally to this work.

https://doi.org/10.1016/j.neuint.2020.104870
Received 15 June 2020; Received in revised form 17 September 2020; Accepted 2 October 2020
Available online 7 October 2020

seizures through the use of a rodent seizure model (Löscher, 2017). Although rodents have long been genetically tractable models of epilepsy research, new model organisms are required due to the practical difficulties of accessing the rodent brain and the limitations of large-scale screening. Within the last few years, zebrafish has become a more easily applicable model organism for drug discovery, including for ASDs (Cunliffe, 2016). Thousands of embryos/larvae can be exposed to chemicals in multi-well plates to test the potential efficacy and teratogenicity/toxicity of known or novel compounds (Phillips and Westerfield, 2014). Moreover, epilepsy-associated sequence variants in hundreds of genes have been identified by genetic analysis, such as genome-wide association studies (GWAS) and exome sequencing studies (Cunliffe, 2016). Therefore, zebrafish are being increasingly leveraged to establish suitable disease models for the development of new clinical tools and the treatment of human diseases (Phillips and Westerfield, 2014).

Since demonstrating the anti-seizure effect of trimethadione in 1944, pentylenetetrazole (PTZ) has been used experimentally to define the seizure phenotype and to identify ASDs using an animal model (Everett and Richards, 1944). The PTZ-induced seizure model in zebrafish is well established and shows behavioral and electrographic seizure activities (Baraban et al., 2005). Zebrafish *scn1lab* mutants, a model of Dravet syndrome, which is catastrophic paediatric epilepsy with severe intellectual disability, exhibit spontaneous abnormal electrographic activity, hyperactivity and convulsive behaviors (Baraban et al., 2013). Zebrafish *zc4h2* knock-out (KO), a model for Miles-Carpenter syndrome (MCS) in which epileptic seizures and intellectual disabilities occur, exhibit abnormal swimming and defective pectoral fin contractures (Frints et al., 2019; May et al., 2015).

In this study, we performed a phenotype-based screening of 6,566 small molecules to identify a novel anti-seizure effective molecule using the zebrafish *zc4h2* KO model. We selected 4-(2-chloro-4-fluorobenzyl)-3-(2-thienyl)-1,2,4-oxadiazol-5(4H)-one (hereafter referred to as GM-90432) as an ASD hit and assessed its efficacy in PTZ-induced zebrafish and mouse seizure models. In addition, GM-90432 effectively reduced seizure-like events through electroencephalogram (EEG) analysis. We also characterized the mode of action of GM-90432 in acutely isolated rat hippocampal CA3 pyramidal neurons using a patch-clamp system. Finally, we characterized GM-90432 as a potential ASD through pharmacokinetic analysis. Taken together, we demonstrated that GM-90432 effectively ameliorates seizure behaviors in animal models and plays a role in neuronal voltage-gated Na^+ channels to exert its anti-seizure efficacy.

2. Materials and methods

2.1. Animal experiments

Zebrafish were maintained under standard conditions as previously described (Westerfield, 2000). ICR mouse purchased from a company producing laboratory animals (Orient Bio Inc., Republic of Korea). All experimental procedures involving zebrafish were performed in accordance with the NIH guide for the care and use of Laboratory Animals (No.8023, amended in 1996). Also, experimental procedure involving mouse was approved by the Animal Care and Use Committee of the Korea Research Institute of Chemical Technology (2019-7B-08-02).

2.2. Evaluation of anti-seizure effects in zebrafish seizure model

At 5 day-post fertilization (dpf), *zc4h2* KO larvae showing loss of swim bladder and ventrally curved body were collected placed a individuals per well in 96-well plate with 100 μl of egg water (EW, 60 μg/ml of Sea salt (S9883; Sigma-Aldrich, St. Louis, MO) in distilled water). 100 μl of DMSO and GM-90432 (final concentrations are 5, 10, and 20 μM) were added into each wells. After exposure for 30 min, single larva was mounted on 5% methyl cellulose and recorded movements of pectoral fins and jaw for 10 s. At 5 dpf, healthy zebrafish larvae were collected and placed 1 individual per well in 96-well plate with 100 μl of EW. They were maintained in a quiet environment from morning until afternoon. 100 μl of DMSO and GM-90432 (final concentrations are 0.5, 1, and 2 μM) were added into each wells with or without pentylenetetrazole (PTZ, P6500; Sigma-Aldrich). The locomotor activity of each larvae was recorded using EthoVision XT software (Noldus, Wageningen, Netherlands) connected to DanioVision chamber (Noldus) for 30 min.

2.3. Whole-mount immunohistochemistry

Whole-mount immunohistochemistry for ERK and phosphorylated ERK was conducted as previously described (Randlett et al., 2015). In the morning of 5 dpf, larvae were arrayed into a 12-well plate with mesh sieve (3478; Corning Inc., Corning, NY) to ensure rapid fixation. They were maintained in a quiet environment until afternoon. DMSO and 2 μM GM-90432 were added into each wells with or without PTZ. After 30 min, each mesh sieve were immediately transferred into 4% paraformaldehyde. After overnight fixation, all steps for immunohistochemistry were proceeded according to Randlett et al. The total ERK antibody (#4696; Cell signaling Technology, Danvers, MA) and phosphorylated ERK antibody (#4370; Cell signaling Technology) were used as a primary antibody. Goat anti-Rabbit IgG (A-11034; Invitrogen, Carlsbad, CA) and Goat anti-mouse IgG (A32727; Invitrogen) were used as a secondary antibody. Images were acquired and quantified using the Lionheart FX automated microscope (BioTek, Winooski, VT) and Gen5 Image Prime (Ver. 3.08).

2.4. EEG analysis in adult zebrafish

Eugenol (Sigma-Aldrich) was used for anesthesia in 7.5 ppm oral administration and 15 ppm bath exposure (Cho et al., 2017; Grush et al., 2004). Zebrafish were exposed in 15 ppm eugenol bath until stage 3 anesthesia was induced and then 7.5 ppm eugenol was orally administrated to maintain zebrafish out of water. All chemicals were dissolved in DMSO concentration of 1% v/v and given by the ollay administration. PTZ was used as a convulsant and treated in 220 mg/kg concentration (Banote et al., 2013). PTZ (220 mg/kg) and GM-90432 (12.5, 25, and 50 mg/kg) were co-treated. All zebrafish were euthanatized by ice water (0–4 °C) at least 10 min after experiment. After stage 3 anesthesia in 15 ppm bath exposure, zebrafish were put in a customized trapping platform to immobilize the animals out of water during EEG recording, during which 7.5 ppm eugenol was orally administrated continuously. A non-invasive EEG electrode was placed on the head skin, above the telencephalon (Cho et al., 2017). The baseline recording session was for 5 min and then, after drug administration, the EEG recording session for 25 min followed. Seizure-like events were manually counted, and Fast Fourier Transform was conducted to extract the power amount of brain signals (Veauthier, 2009). All EEG recording was performed using Biopac Student Lab 4.1 (Biopac Systems, Inc., Goleta, CA). To investigate the effect of drugs on brain signals quantitatively, the relative power of brain signals before and after drug administration was compared with the following equation:

$$\frac{Amount\ of\ power(Treated) - Amount\ of\ power(Baseline)}{Amount\ of\ power(Baseline)} \times 100(\%)$$

We selectively compared the power of signals in the frequency range from 0 to 16 Hz using FIJI (ImageJ) software.

2.5. Evaluation of anti-seizure effects in mouse seizure model

7-weeks old ICR male mice were kept in plastic case with free access to food and water. The animal room was maintained at 23 ± 3 °C, relative humidity of 50 ± 10% with approximately 12 h dark/light cycle. 50 mg/kg of GM-90432 and dosing vehicle were used as DMSO,

PEG400, and deionized water (5:70:25, v/v/v) for intraperitoneal (I.P.) injection. After 30 min, 60 mg/kg of PTZ were administrated by I.P. injection. Then, behaviors of mouse was recorded using video camera for 10 min. Frequency of seizure-like behaviors were assessed through recorded media at intervals of 10 s according to modified Racine's scale (Fig. 4A).

2.6. Electrophysiology

Sprague Dawley rats (12–17 day-old, either sex) were decapitated under ketamine anesthesia (50 mg/kg, i.p.). The brain was dissected and transversely sliced at a thickness of 400 μm using a microslicer (VT1000S; Leica, Nussloch, Germany). Slices containing the hippocampus were kept in an incubation medium (in mM; 124 NaCl, 3 KCl, 1.5 KH_2PO_4, 24 $NaHCO_3$, 2 $CaCl_2$, 1.3 $MgSO_4$ and 10 glucose) saturated with 95% O_2 and 5% CO_2 at room temperature (22–25 °C) for at least 1 h before the mechanical dissociation. For dissociation, slices were transferred into a 35 mm culture dish (Primaria 3801; Becton Dickinson, Rutherford, NJ), which contained a standard external solution (in mM; 150 NaCl, 3 KCl, 2 $CaCl_2$, 1 $MgCl_2$, 10 glucose and 10 HEPES, a pH of 7.4 with Tris-base), and the hippocampal CA3 region was identified under a binocular microscope (SMZ-1; Nikon, Tokyo, Japan). Details of the mechanical dissociation have been described previously (Akaike and Moorhouse, 2003; Jang et al., 2006). Electrical measurements were performed using conventional whole-cell patch recordings and a patch-clamp amplifier (Axopatch 200B; Molecular Devices, Union City, CA) with a K^+-free external solution (in mM; 130 NaCl, 20 tetraethylammonium-Cl, 3 CsCl, 2 $CaCl_2$, 1 $MgCl_2$, 10 glucose, and 10 HEPES, and was adjusted to pH 7.4 with Tris-base). Neurons were voltage clamped at a holding potential (VH) of −100 mV, except where indicated. Patch pipettes were made from borosilicate capillary glass (G-1.5; Narishige, Tokyo, Japan) using a pipette puller (P-97; Sutter Instrument Co., Novato, CA). The resistance of the recording pipettes filled with the internal solution (in mM; 140 CsF, 10 CsCl, 2 EGTA, 2 ATP-Na_2, and 10 HEPES with the pH adjusted to 7.2 with Tris-base) was 1.0–1.5 MΩ. Membrane currents were filtered at 3 kHz, digitized at 10 kHz, and stored on a computer equipped with pCLAMP 10.6 (Molecular Devices). Capacitative and leakage currents were subtracted by the P/4 protocol using pCLAMP program. During recordings, 10 mV hyperpolarizing step pulses (30 ms in duration) were periodically applied to monitor the access resistance, and recordings were discontinued if access resistance changed by more than 10%. To record voltage-gated Na^+ currents (I_{Na}), the K^+-free external solution routinely contained 100 μM Cd^{2+} to block voltage-gated Ca^{2+} channels. Depolarizing step pulses to evoke the I_{Na} were applied with an interval of 10 s (except where indicated), which was sufficiently long enough to recover from the inactivation of voltage-gated Na^+ channels. All solutions containing drugs were applied using the "Y-tube system" for rapid solution exchange (Murase et al., 1989). All experiments were performed at room temperature (22–25 °C). The amplitude of I_{Na} was measured by subtracting the baseline from the peak amplitude of I_{Na} by using pCLAMP 10.6. The voltage-inactivation relationship of Na^+ channels were fitted to the Boltzmann equations; $I/I_{max} = 1–1/\{1 + \exp[(V_{50} – V)/k]\}$, where I_{max} are the maximum current amplitude, V_{50} are half-maximal potentials for fast inactivation, and k is the slope factor. The kinetic data for the development of inactivation and the recovery from inactivation were fitted to the following equations; $I(t) = A_0 + A_{fast}$ x $[\exp(–t/\tau_{fast})] + A_{slow}$ x $[\exp(–t/\tau_{slow})]$, and $I(t) = A_0 + A_{fast}$ x $[1 – \exp(–t/\tau_{fast})] + A_{slow}$ x $[1 – \exp(–t/\tau_{slow})]$, respectively, where $I(t)$ is the amplitude of I_{Na} at time t, and A_{fast} and A_{slow} are the amplitude fraction of τ_{fast}, and τ_{slow}, respectively.

2.7. Pharmacokinetic studies in mouse

Pharmacokinetic studies of GM-90432 was performed on 7-weeks old ICR male mouse. Different dose and dosing vehicle were used as DMSO, PEG400, and deionized water (5:40:55, v/v/v) for intravenous (I.V.) injection (5 mg/kg, 5 mL/kg), and DMSO, PEG400, and deionized water (5:70:25, v/v/v) for I.P. injection (50 mg/kg, 5 mL/kg) according to physicochemical properties of GM-90432. For plasma concentration-time profiles of GM-90432, blood samples were collected at 0.083, 0.5, 1, 2, 4, and 8 after drug administration. For calculation of blood to plasma (B/P) ratio of GM-90432 in male mouse, blood and brain tissues were collected at 0.5 h after I.P. injection of GM-90432 (50 mg/kg). The blood samples were immediately centrifuged at 15,000 RPM for 3 min, to collect plasma samples. Plasma and brain homogenates were extracted by adding nine volume of acetonitrile. After vortexing for 10 min, the samples were centrifuged at 15,000 RPM for 10 min at 4 °C, and then 100 μL of clear supernatant was transferred to LC vial and analyzed by Liquid chromatography mass spectrometry (LC-MS/MS). The plasma concentration-time profiles for pharmacokinetic evaluation of GM-90432 were analyzed by non-compartmental method using the nonlinear least squares regression program WinNonlin 5.3 (Pharsight, Mountain View, CA, USA). The area under the plasma concentration–time curve from time zero to the final point (AUC_h) and the area from time zero to infinite time (AUC_{inf}) by adding extrapolated area were calculated using the trapezoidal rule. The terminal elimination half-life ($t_{1/2}$), total clearance (CL), and apparent volume of distribution at steady state (V_{ss}) for GM-90432 were determined using individual plasma concentration–time profiles.

2.8. Pharmacokinetic studies in zebrafish

Chemical uptake study of GM-90432 was performed on 5 dpf zebrafish larvae. The larvae were exposed to 5 μM of GM-90432 for 5, 10, 30, and 60 min. After drug exposure, zebrafish larvae, larval medium, blank medium (without zebrafish larvae) were collected in 1.7 mL tube. The fishes were extracted by adding 500 μL of methanol, and homogenized using sonicator. The samples were centrifuged at 15,000 RPM for 10 min at 4 °C and analyzed by LC-MS/MS. For calculation of B/P ratio of GM-90432 in adult zebrafish (11 months-old), blood and brain tissues were collected at 0.5 h after oral administration (P.O.) of GM-90432 (50 mg/kg). The blood samples and brain samples were analyzed by LC-MS/MS.

2.9. Statistical analysis

All statistical analysis was performed on Prism 8.4.3 (GraphPad, La Jolla, CA). Numerical values are provided as the mean ± S.E.M. (Standard Error of Mean). Zebrafish and mouse results were analyzed using unpaired two-tailed *t*-test and Brown-Forsythe and Welch analysis of variance (ANOVA). Significant differences in the mean amplitude were tested using Student's paired two-tailed *t*-test with absolute values rather than normalized ones. Values of $p < 0.05$, $p < 0.01$ and $p < 0.001$ were considered significantly different.

3. Results

3.1. Anti-seizure effects of GM-90432 in zebrafish seizure models

A total of 6,566 small molecules provided by the Korea Chemical Bank were screened for their anti-seizure efficacy at a concentration of 20 μM using *zc4h2* KO larvae (Fig S1). At 5 dpf, *zc4h2* KO larvae exhibited continuous swimming movements and balance problems compared with wild-type siblings (May et al., 2015). The efficacy of the anti-seizure therapy was defined as decreased active movements in *zc4h2* KO larvae and unchanged movements in wild-type siblings for 30 min. Among the 6,566 molecules, more than 8 compounds were observed to have anti-seizure effects without toxicity, such as heart arrest (Fig S1). Finally, GM-90432 was identified as a prototype (Fig. 1A). At 5 dpf, *zc4h2* KO larvae also exhibited active movements of the pectoral fins and jaw compared with wild-type sibling (May et al., 2015). To

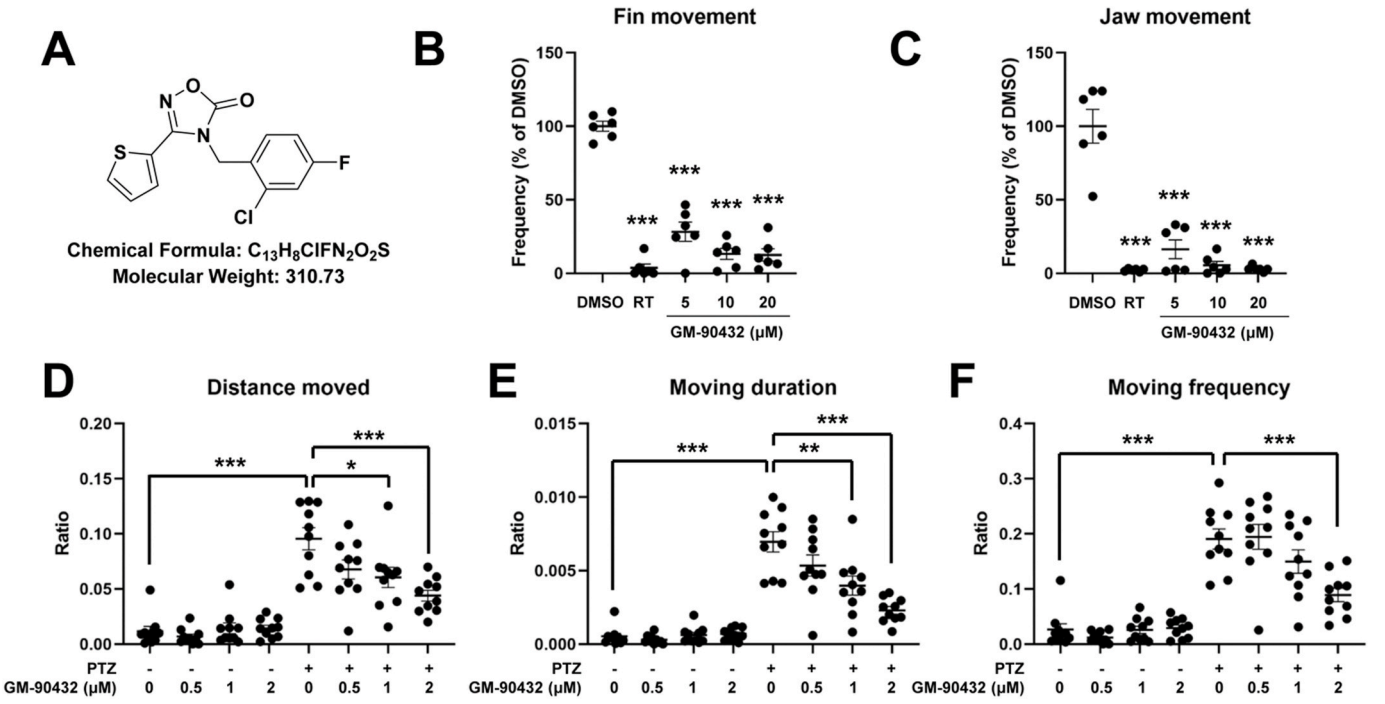

Fig. 1. Anti-seizure effects of GM-90432 in a zebrafish seizure model. (A) Chemical structure of GM-90432. (B) Pectoral fin movement and (C) jaw movement were assessed in *zc4h2* KO larvae with DMSO, retigabine (RT), and GM-90432 treatments. n = 6. (D) Distance moved, (E) moving duration, and (F) moving frequency were quantified as seizure-like behaviours to assess GM-90432 effects in PTZ-induced zebrafish larvae. The value was quantified as a high speed (above 80 mm/s)/ total movement ratio. n = 10.

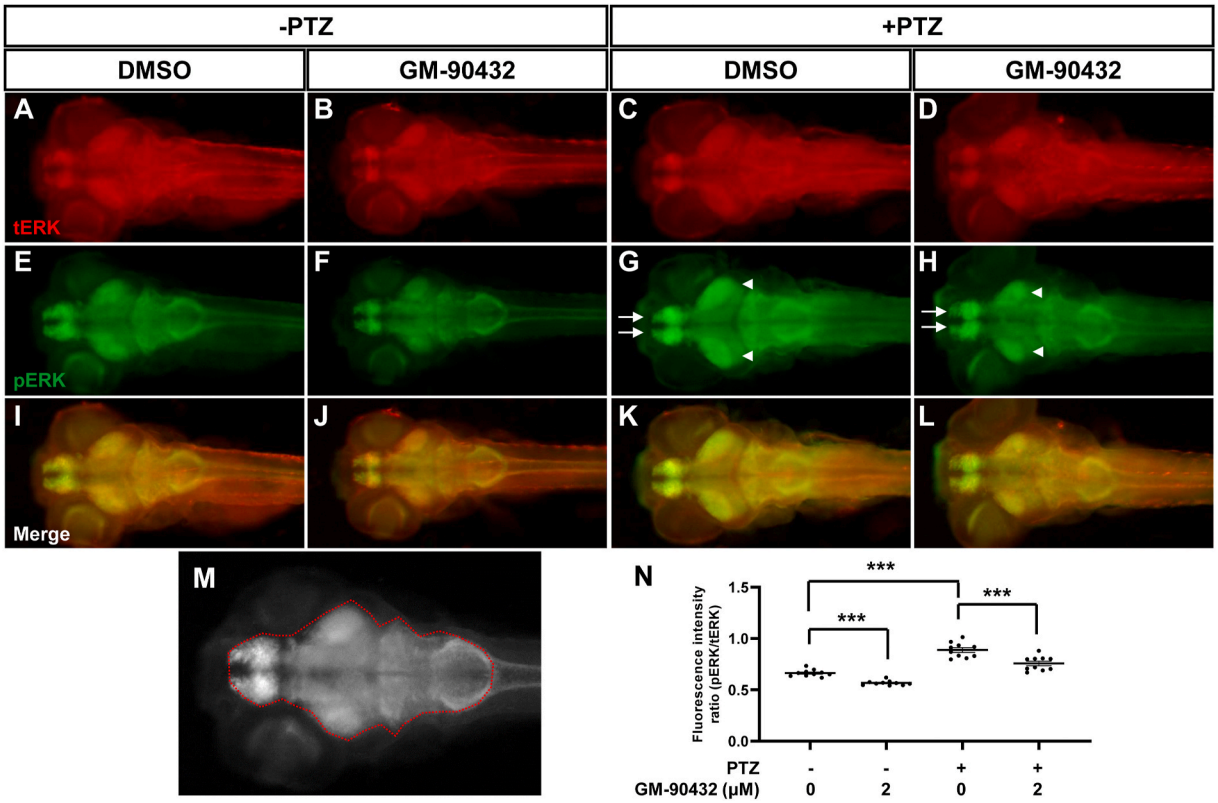

Fig. 2. Whole-mount immunohistochemistry for tERK and pERK in PTZ-induced seizure zebrafish larvae. Representative images of immunohistochemistry for (A–D) total ERK/MAPK (tERK), (E–H) phosphorylated ERK (pERK), and (I–L) merge. (A, E, I) DMSO treatment and (B, F, J) 2 μM GM-90432 treatment without PTZ treatment. (G, C, K) DMSO treatment and (D, H, L) 2 μM GM-90432 treatment in PTZ-induced zebrafish larvae. Arrows and arrowheads indicate the telencephalon and optic tectum, respectively. (M) Representative image of larvae. Red dash line indicates brain region to quantify fluorescence intensity. (N) Quantification of fluorescence intensity ratio for pERK/tERK. n = 10.

determine whether these hyperactivities were inhibited by GM-90432, *zc4h2* KO larvae exposed to GM-90432 or retibagine, an anti-convulsant (Patsalos and Berry, 2012), were used as an adjunctive treatment for partial epilepsy for 30 min. As a positive control, 5 μM retigabine treatment reduced pectoral fin and jaw movements in *zc4h2* KO larvae (Fig. 1B and C). GM-90432 treatment also effectively reduced fin and jaw active movements in *zc4h2* KO larvae (Fig. 1B and C). Next, we assessed the anti-seizure efficacy of GM-90432 in PTZ-induced zebrafish larvae to verify the reproducibility within each model. PTZ-induced zebrafish have well-established seizure phases in larvae: dramatic increase in locomotor activity (stage 1), rapid "whirlpool-like" circling behavior (stage 2), and loss of posture (stage 3) (Baraban et al., 2005). In this study, we established new methods for inducing and quantifying seizures by PTZ induction. Because PTZ irregularly and dramatically increased locomotor activity in zebrafish larvae, we quantified the behavioral parameters according to the high speed of 40, 60, 80, or 100 mm/s. The behavioral parameters defined the distance moved, moving duration, and moving frequency as a high speed/total movement ratio. As a result, the behavioral parameters significantly increased compared with the control group at a 5 mM concentration of PTZ and a speed above 80 mm/s (Fig. S2). Next, we exposed zebrafish larvae to GM-90432 in 5 mM PTZ and quantified the high/total movement ratio at speeds above 80 mm/s. Indeed, 2 μM GM-90432 effectively restored the distance moved, moving duration, and moving frequency compared with the PTZ-only treated group, whereas GM-90432 treatment groups without PTZ did not change behavioral parameters (Fig. 1D–E).

Next, we performed whole-mount immunohistochemistry for phosphorylated extracellular signal-regulated kinase (pERK) to demonstrate neural activity in GM-90432-treated zebrafish larvae. pERK is a more permissive endogenous sensor than immediate early genes (IEGs), such as *c-fos* and *arc*, and an improved marker for neural activity (Randlett et al., 2015). Staining for pERK in PTZ-treated larvae exhibited enrichment in the nervous system, with the strongest staining in the telencephalon and optic tectum. However, GM-90432 treatment in PTZ-induced larvae significantly reduced pERK in the telencephalon and optic tectum. In addition, total ERK/MAPK (tERK) did not change in any of the experimental groups (Fig. 2, S7). These results demonstrated that GM-90432 effectively restored behavioral phenotypes and neural activities in PTZ seizure-induced zebrafish larvae.

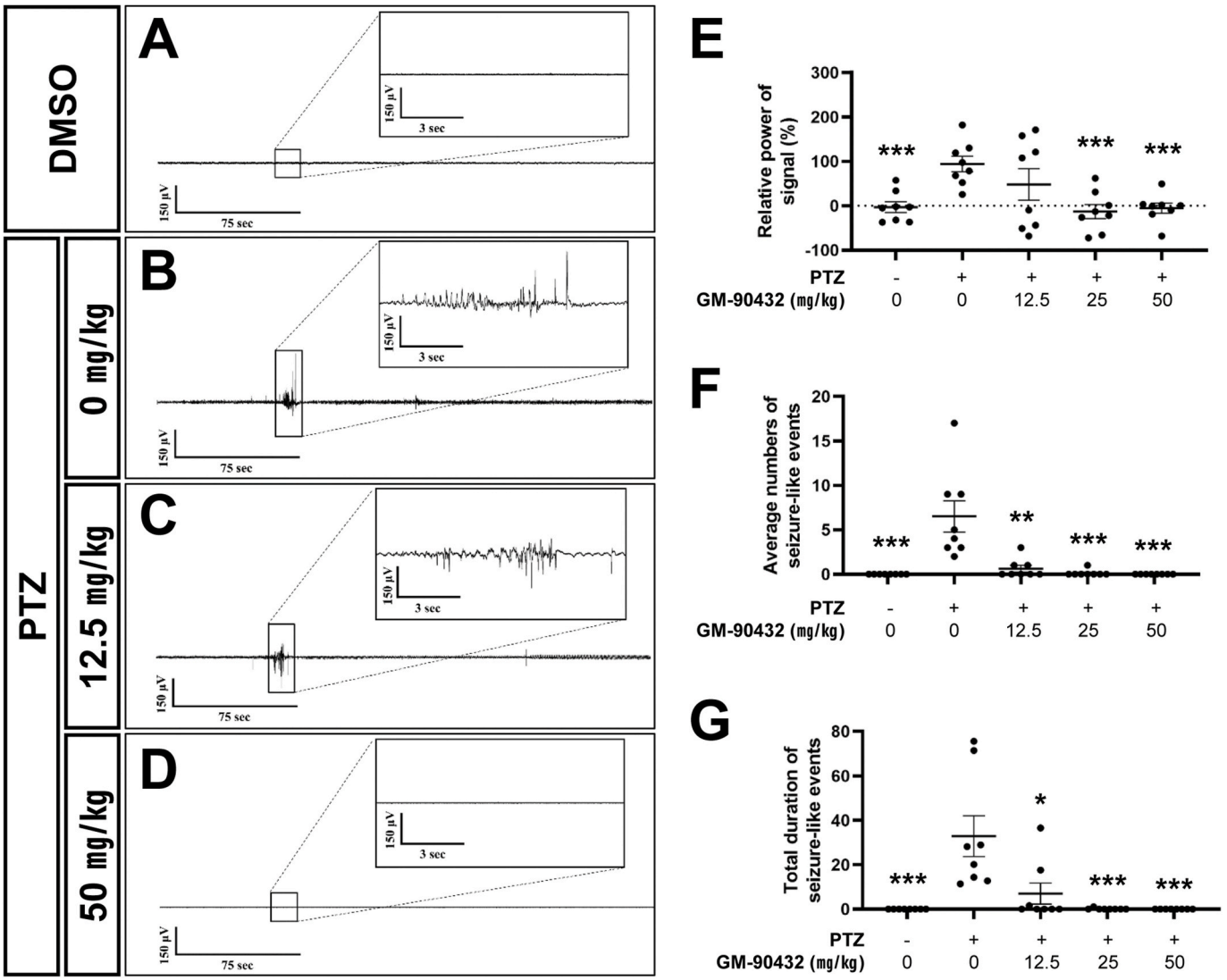

Fig. 3. Electroencephalogram (EEG) analysis in PTZ-induced adult zebrafish. Seizure-like events are distinguishable from normal brain signals in real-time EEG data of zebrafish. (A) The baseline was recorded for 5 min with no other chemical treatment except for eugenol for anesthesia. (B) Seizure-like events were detected after PTZ treatment. (C) At 12.5 mg/kg GM-90432 dose administration, three out of a total of 8 zebrafish displayed seizure-like events after administration. (D) After 50 mg/kg GM-90432 treatment, no seizure-like events were detected in contrast to PTZ treatment. (E) The relative power of the signal, (F) the average number of seizure-like events and (G) the total duration of seizure-like events were compared among the differently treated groups. n = 8.

3.2. Electroencephalogram (EEG) analysis of adult zebrafish

EEG is widely considered a prominent diagnostic tool for detecting epilepsy (Gandhi et al., 2010; Tzallas et al., 2009). Neither seizure-like events nor abnormal spikes appeared in the baseline recording in the DMSO-treated group (Fig. 3A). In contrast, abnormal spikes were detected in the PTZ-induced epilepsy model (Fig. 3B). Such seizure-like events have been reported to be commonly detected in the PTZ model in previous research (Afrikanova et al., 2013; Cho et al., 2017). Seizure-like events were observed over the entire recording session (Fig. 3B). Thus, the presence of seizure-like events in real-time recorded EEG data is crucial to determine the epilepsy state (Afrikanova et al., 2013). In this regard, the number of seizure-like events that occurred in PTZ and GM-90432 co-treated zebrafish supports the reliability of AED screening efficacy. After 12.5 mg/kg GM-90432 dose administration, seizure-like events were still observed in three out of 8 zebrafish (Fig. 3C). However, a 50 mg/kg dose was considered a sufficient dose to protect the animals from PTZ (Fig. 3D).

After treatment with PTZ, the relative power of the signal significantly increased. PTZ administration clearly induced seizures and increased the signal power of the brain. No difference was observed between the 25 and 50 mg/kg dose GM-90432 groups and the DMSO-treated group, while there was a significant difference between these two groups and the PTZ-treated group. When GM-90432 at concentrations of 25 and 50 mg/kg were co-treated with PTZ, the efficacy as an anti-seizure agent was confirmed by measuring the relative power of the signal. One-way ANOVA suggested no significant difference between the 12.5 mg/kg dose group and the PTZ-treated group (Fig. 3E). During the 25-min recording session after PTZ injection, a significant number of seizure-like events were detected. There were no seizure-like events detected in the DMSO-treated group or the 50 mg/kg dose group. After 25 mg/kg dose administration, seizure-like events were detected in only one out of a total of 8 zebrafish in the same group. Additionally, seizure-like events were detected in three out of a total of 8 zebrafish in the 12.5 mg/kg dose group. Although seizure-like events were observed in both the 12.5 and 25 mg/kg dose groups, no significant difference was found compared to the DMSO-treated group. Compared to the PTZ-treated group, DMSO and all three dose groups showed significant differences in the average number of seizure-like events (Fig. 3F). As discussed in Fig. 3F, no seizure-like events were found in the DMSO-treated group or the 50 mg/kg dose group. The total duration of seizure-like events significantly increased in the PTZ-treated group and slightly increased in the 12.5 and 25 mg/kg dose groups (Fig. 3G). Similar to Fig. 3F, there was no significant difference between the 12.5 and 25 mg/kg dose groups and the DMSO-treated group, but the differences were significant when compared to the PTZ group (Fig. 3G).

3.3. Anti-seizure effects of GM-90432 in PTZ-induced mice

It has been well established that seizure-induced rodent models are associated with obvious behaviors (Racine, 1972). To determine whether GM-90432 restores seizure-like behaviors in rodents, we

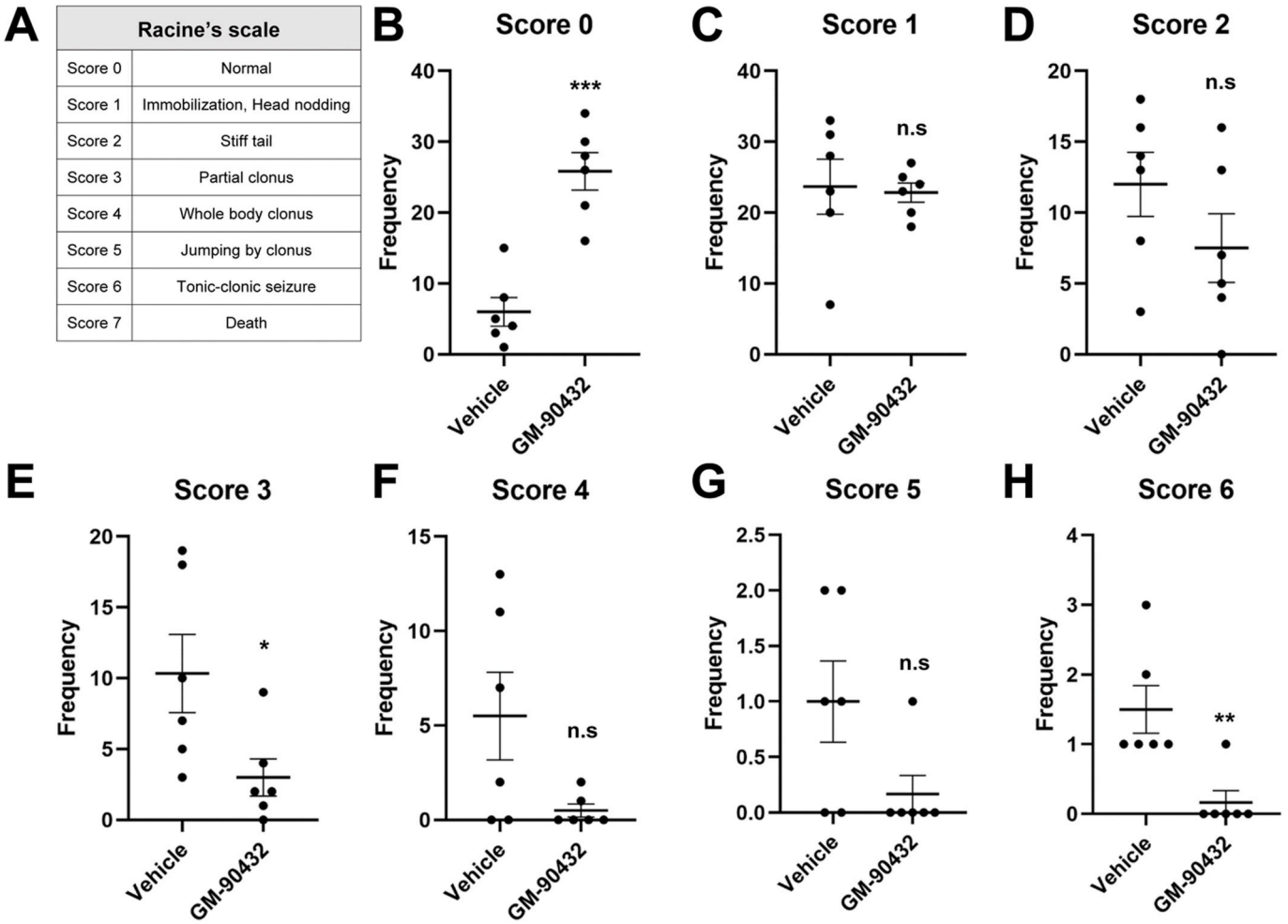

Fig. 4. Anti-seizure effects of GM-90432 in PTZ-induced seizure mice. (A) Modified Racine's scale. (B) score 0: normal behaviour, (C) score 1: immobilization and head nodding, (D) score 2: stiff tailing, (E) score 3: partial clonus, (F) score 4: whole body clonus, (G) score 5: jumping by clonus, and (H) score 6: tonic-clonic seizures were quantified as seizure-like behaviours to assess GM-90432 effects in single PTZ-induced mice. n = 6.

introduced GM-90432 in single PTZ-induced seizure mice and assessed seizure-like behaviors using a modified Racine's scale (Fig. 4A) (Dhir, 2012). According to the modified Racine's scale, GM-90432 effectively restored seizure-like behaviors in PTZ-induced seizure mouse as follows: score 0: GM-90432 significantly recovered normal behaviors (6.0 ± 4.98 for the vehicle and 25.83 ± 6.46 for GM-90432, Fig. 4B); scores 1 and 2: immobilization/head nodding and stiff tailing behaviors did not change between the vehicle and GM-90432 (Fig. 4C and D); score 3: partial clonus behavior was effectively decreased by GM-90432 administration (10.33 ± 6.74 for the vehicle and 3.0 ± 3.22 for GM-90432, Fig. 4E); scores 4 and 5: whole body clonus and jumping by clonus behaviors showed decreased patterns after GM-90432 administration (5.50 ± 5.68 for the vehicle and 0.50 ± 0.84 for GM-90432 in score 4, $p = 0.058$; 1.0 ± 0.89 for the vehicle and 0.17 ± 0.41 for GM-90432 in score 5, Fig. 4F and G)); score 6: tonic-clonic seizures were decreased by GM-90432 administration (1.50 ± 0.84 for the vehicle and 0.17 ± 0.41 for GM-90432, Fig. 4H)); score 7: no mice died in this experiment. Taken together, these results demonstrated that GM-90432 effectively restored seizure-like behaviors in single PTZ-induced seizure mice.

3.4. Effects of GM-90432 on voltage-gated Na^+ channels in hippocampal CA3 neurons

Since voltage-gated Na^+ channels are key ion channels involved in neuronal excitability, a number of drugs that modulate these ion channels are widely used for the treatment of epilepsy (Catterall, 2014; Macdonald and Kelly, 1995). Therefore, we examined the effect of GM-90432 on voltage-gated Na^+ channels using a whole-cell patch clamp technique. The voltage-gated Na^+ currents (I_{Na}) were recorded from acutely isolated hippocampal CA3 pyramidal neurons by applying brief depolarizing step pulses (−100 to −20 mV, every 5 s). Application of GM-90432 (100 μM) elicited a small but significant decrease in the I_{Na} (92.9 ± 2.0% of the control, Fig. 5A). We also examined the effect of GM-90432 on the voltage-inactivation relationship of voltage-gated Na^+ channels. The I_{Na} was induced by test pulses (−20 mV, 50 ms duration) followed by conditioning prepulses (−120 to −20 mV in 10 mV increments, 500 ms duration). The peak amplitudes of I_{Na} observed in the absence and presence of 100 μM GM-90432 were normalized to the maximal amplitude of I_{Na} and fitted to the Boltzmann function (Fig. 5C). GM-90432 (100 μM) significantly shifted the V_{50} towards hyperpolarizing ranges (−2.9 ± 0.4 mV shift), where the V_{50} values were −61.2 ± 1.8 mV for the control and −64.1 ± 1.6 mV after GM-90432 treatment (Fig. 5D).

Next, we examined the effect of GM-90432 on the inactivation kinetics of voltage-gated Na^+ channels using a two-pulse protocol, which is composed of the first conditioning pulses (P_1, -100 to −20 mV, 2–8,000 ms duration) and the subsequent second test pulse (P_2, -100 to −20 mV, 50 ms duration) with an interpulse interval of 20 ms. The ratios of the two currents (P_2/P_1) calculated in the absence and presence of 100 μM GM-90432 were plotted against the duration of the conditioning pulses and then fitted to a double exponential function (Fig. 5E). The resultant fast and slow time constants (τ_{fast} and τ_{slow}) represent the fast and slow components for the onset of inactivation of voltage-gated Na^+ channels. GM-90432 (100 μM) significantly decreased τ_{fast} (1,168.8 ± 92.9 ms for the control and 664.5 ± 111.7 ms after GM-90432 treatment, Fig. 5F). However, τ_{slow} was not affected by GM-90432 (4,860.3

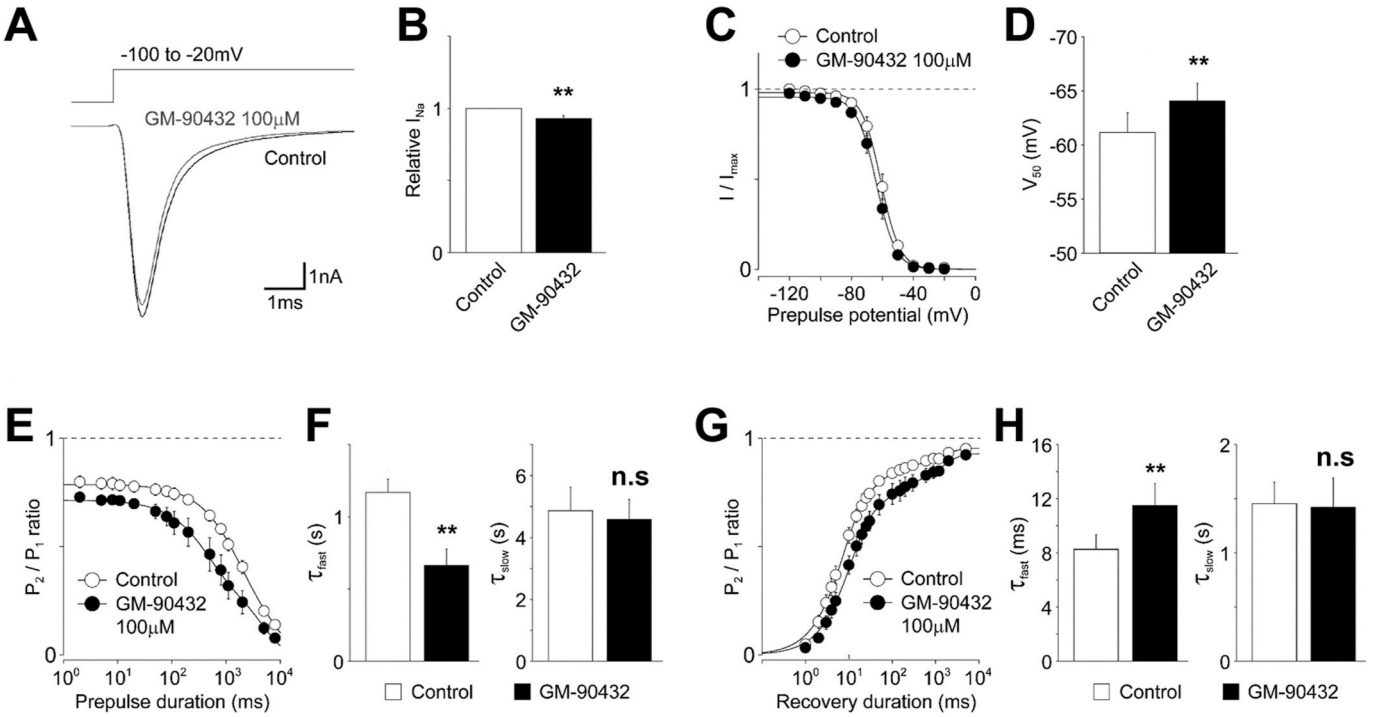

Fig. 5. Effects of GM-90432 on voltage-gated Na^+ channels. (A) Typical traces of voltage-gated I_{Na} in the absence and presence of 100 μM GM-90432. I_{Na} was elicited by electrical stimulation from a holding potential of −100 mV to −20 mV (100 ms duration) every 5 s (0.2 Hz). (B) Change in the peak amplitude of voltage-gated I_{Na} by 100 μM GM-90432. Each column represents the mean and S.E.M. from 12 experiments. (C) Current-voltage relationships of voltage-gated Na^+ channels in the absence (open circles) and presence (closed circles) of 100 μM GM-90432. Continuous lines represent the best fit of the Boltzmann function. Each point represents the mean and S.E.M. from 4 experiments. (D) GM-90432-induced changes in the midpoint voltage for inactivation (V_{50}) of voltage-gated Na^+ channels. Each column represents the mean and S.E.M. from 4 experiments. (E) Kinetics for the onset of inactivation of voltage-gated Na^+ channels in the absence (open circles) and presence (closed circles) of 100 μM GM-90432. Each point represents the mean and S.E.M. from 6 experiments. (F) GM-90432 (100 μM)-induced changes in the fast (τ_{fast}, left) and slow (τ_{slow}, right) time constants for the onset of inactivation of voltage-gated Na^+ channels. Each column represents the mean and S.E.M. from 6 experiments. (G) Kinetics for the recovery from inactivation of voltage-gated Na^+ channels in the absence (open circles) and presence (closed circles) of 100 μM GM-90432. Each point represents the mean and S.E.M. from 7 experiments. (H) GM-90432 (100 μM)-induced changes in the fast (τ_{fast}, left) and slow (τ_{slow}, right) time constants for the recovery from inactivation of voltage-gated Na^+ channels.

± 758.5 ms for the control and 4,575.1 ± 654.6 ms after GM-90432 treatment, Fig. 5F). We also examined the effect of GM-90432 on the recovery kinetics of voltage-gated Na^+ channels using a two-pulse protocol, which is composed of the first conditioning pulses (P_1, -100 to −20 mV, 500 ms duration) and the subsequent second test pulse (P_2, -100 to −20 mV, 50 ms duration) with various interpulse intervals (1–5,000 ms). The P_2/P_1 ratios calculated in the absence and presence of 100 μM GM-90432 were plotted against the duration of recovery time and then fitted to a double exponential function (Fig. 5G). The resultant τ_{fast} and τ_{slow} represent the fast and slow components for the recovery from the inactivation of voltage-gated Na^+ channels. GM-90432 (100 μM) significantly increased τ_{fast} (8.3 ± 1.1 ms for the control and 11.5 ± 1.6 ms after GM-90432 treatment) but not τ_{slow} (1,454.8 ± 198.7 ms for the control and 1,422.2 ± 271.3 ms after GM-90432 treatment, Fig. 5H).

3.5. Pharmacokinetic characterization of GM-90432

The quantitative analysis of GM-90432 was performed on a C18 column using liquid chromatography mass spectrometry in APCI + mode. To calculate pharmacokinetic parameters, including bioavailability and T_{max} (time to maximum plasma concentration), plasma concentration-time profiles of GM-90432 were investigated in 7-week-old mice following I.V. (5 mg/kg) or I.P. (50 mg/kg) injection (Fig. 6A). The estimated pharmacokinetic parameters of GM-90432 are summarized in Table 1. The absolute bioavailability of GM-90432 was estimated to be 31.2%. Additionally, GM-90432 was rapidly absorbed into fish bodies in an exposure time-dependent manner in 5 dpf zebrafish larvae (Fig. 6B). Furthermore, blood-brain barrier (BBB) penetration studies were performed to estimate the B/P ratio (brain to blood or plasma concentration ratio) values of GM-90432 in mouse and zebrafish models following I.P. injection or oral administration of GM-90432 for 0.5 h, respectively. The values were determined to be 1.70 ± 0.07 in adult mice and 2.13 ± 0.34 in adult zebrafish, indicating that GM-90432 has BBB-permeable properties in both models (Fig. 6C). Furthermore, the Caco-2 cell permeability assay showed an apparent permeability (P_{app}) of 33.5 × 10^{-6} cm/s in absorption/uptake and 44.7 × 10^{-6} cm/s in secretion/efflux of GM-90432, suggesting that GM-90432 is highly permeable in human intestinal epithelial cells with an efflux ratio of 1.36 ± 0.26 (Fig. S6).

Table 1
Pharmacokinetic parameters of GM-90432 in mice.

Parameters	I.V. 5 mg/kg	I.P. 50 mg/kg
T_{max} (h)	NA	0.5 ± 0.00
C_{max} (μg/mL)	NA	0.64 ± 0.16
$T_{1/2}$ (h)	1.70 ± 0.33	5.99 ± 1.25
AUC_t (μg·h/mL)	0.84 ± 0.09	2.62 ± 0.38
AUC_∞ (μg·h/mL)	0.92 ± 0.10	2.89 ± 0.37
CL (L/h/kg)	5.47 ± 0.64	NA
V_{ss} (L/kg)	6.70 ± 2.30	NA
F_t (%)	NA	31.2

NA, not applicable.

4. Discussion

Zebrafish are well-established experimental organisms for neurological studies such as epilepsy for models including the chemical (PTZ)-induced seizure model (Baraban et al., 2005) and the genetic mutation seizure model including Dravet syndrome (Baraban et al., 2013) and Miles-Carpenter syndrome (Frints et al., 2019; May et al., 2015). A small molecule screening to identify anti-seizure candidates using *zc4h2* KO larvae was performed in this study for the first time. Because assessment of mitigating seizure-like behaviors in *zc4h2* KO larvae is fast and suitable, we finally selected GM-90432 using this model. GM-90432 significantly decreased seizure-like behaviors at a 5 mM PTZ and above 80 mm/s of speed, whereas GM-90432 treatment alone did not change the behaviors (Fig. 1, S3). In addition, GM-90432 effectively reduced neural activity through a reduction of elevated pERK protein levels by GM-90432 in PTZ-induced larvae (Fig. 2). Seizure-specific EEG signals using a non-invasive single-channel electrode were effectively decreased in PTZ-treated adult zebrafish by GM-90432 treatment (Fig. 3). The other test for anti-seizure effects, the color preference test, was performed to reveal the recovery of cognition ability in PTZ-induced zebrafish larvae. Indeed, blue preference reduced by PTZ treatment was restored by GM-90432 (Fig. S4). This result also suggests the potential that one of the symptoms of a seizure patient, a decrease in cognitive ability, could be recovered by GM-90432.

Voltage-gated Na^+ channels are major targets for a number of commercially available ASDs (Brodie, 2017; Catterall, 2014). In this study, we also found that GM-90432 shifted the V_{50} values towards hyperpolarizing ranges, suggesting the preferential binding of GM-90432 to voltage-gated Na^+ channels at depolarized membrane potentials. The higher affinity to inactivated Na^+ channels would contribute to the anti-epileptic efficacy of GM-90432, as shown previously (Macdonald and Kelly, 1995). The use-dependent inhibition of Na^+ channels is directly related to the repetitive generation of action potentials at higher frequencies (Catterall, 2014; Roy and Narahashi, 1992). Although we found that GM-90432 had little effect on the use-dependent inhibition of Na^+ channels (data not shown), it has been reported that ASDs acting on voltage-gated Na^+ channels have diverse effects on use-dependent inhibition (Backus et al., 1991; Lang et al., 1993). However, since the extent of use-dependent inhibition is quite different among the recording conditions, such as the holding potential, the length and the amplitude of depolarizing stimuli and neuronal population (Lang et al., 1993; Roy and Narahashi, 1992), further study is

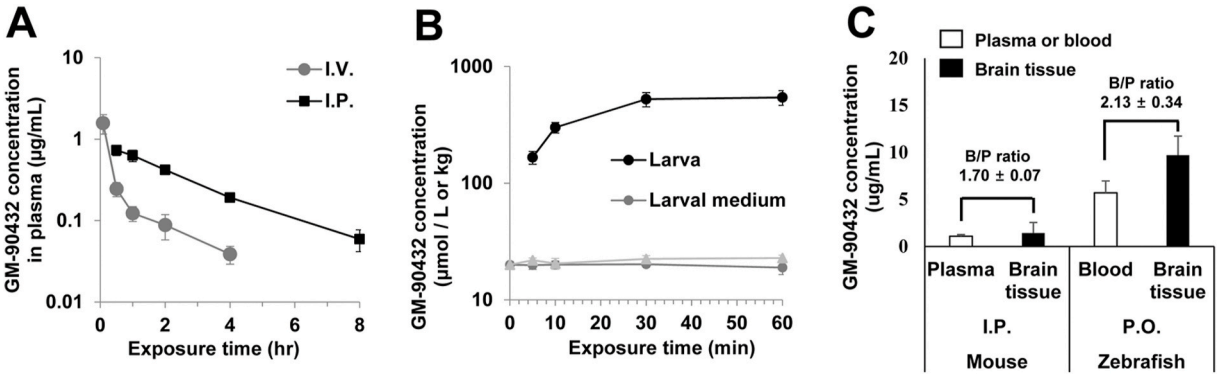

Fig. 6. Pharmacokinetic characterization of GM-90432. Pharmacokinetic analysis of GM-90432 were performed by (A) I.V./I.P. injection in mice (n = 3) and (B) exposure in zebrafish larvae (n = 20). (C) Blood-brain barrier permeability of GM-90432 was analyzed through I.P. injection in mice (n = 3) and P.O. in adult zebrafish (n = 3).

needed to reveal the detailed action of GM-90432 on the use-dependent inhibition of Na^+ channels. The inactivation and recovery kinetics of Na^+ channels also play a pivotal role in the repetitive and bursting generation of action potentials in response to sustained depolarization. In this study, we found that the onset of inactivation and recovery from inactivation of Na^+ channels in CA3 pyramidal neurons were accomplished by two kinetic components, e.g., fast (τ_{fast}) and slow (τ_{slow}),and that GM-90432 affected the fast rather than slow components. The results suggest that GM-90432 accelerates the onset of fast inactivation and retards the fast recovery from inactivation. Such modulation of inactivation and/or recovery kinetics would also contribute to the anti-epileptic efficacy of GM-90432, as other ASDs exhibit similar changes in the inactivation and recovery kinetics of Na^+ channels (Catterall, 2014; Curia et al., 2009; Nakamura et al., 2019). Together, our present results strongly suggest that GM-90432 acts on voltage-gated Na^+ channels to elicit its anti-epileptic efficacy. However, the possibility that GM-90432 acts on other targets cannot be excluded, as ASDs also modulate a number of voltage-gated and ligand-gated ion channels (Armijo et al., 2005; Sills and Brodie, 2001).

Finally, a pharmacokinetic characterization of GM-90432 was undertaken to assess the possibility of developing a therapeutic drug for seizures. Because the central nervous system (CNS) is safely protected by the BBB, which controls the entry of exogenous and endogenous materials into the brain, penetration of drugs into the brain remains one of the main obstacles in the development of drugs (Begley, 1996; Schlossauer and Steuer, 2002). According to FDA approval, a B/P ratio greater than 0.3 is classified as BBB-permeable in the pharmaceutical industry (Reichel, 2006). In addition, there are examples of BBB permeability in zebrafish defined by similar criteria (Kim et al., 2017). Both administration of GM-90432 in mouse and zebrafish showed effective permeation and distribution into the brain (Fig. 6).

5. Conclusion

In summary, we screened small molecules to identify a novel ASD and examined the effects of GM-90432 using zebrafish and mouse seizure models. GM-90432 significantly decreased not only the neural activity but also the seizure-like events on the EEG in PTZ-induced zebrafish. Moreover, electrophysiological analysis revealed that GM-90432 plays a role in voltage-gated Na^+ channels. Taken together with its pharmacokinetic characterization, we suggest that GM-90432 has the potential to be developed into a new ASD candidate.

Author statement

K.-S.H., H.K., S.S.K., J.S.C, J.Y.Y., D.-S.S., and S.H.A. carried out the experiments involved zebrafish and mice. J.-H.C. and I.-S.J involved electrophysiologic study. J.S. and J.J. performed EEG analysis. K.-S.H., H.K. and M.A.B. wrote the manuscript. K.-S.H., J.H.A., C.-H.K. and M. A.B. designed the study.

Declaration of competing interest

The authors declare no conflict of interest.

Acknowledgments

This work was supported by a grants from the Ministry of Trade, Industry and Energy (2020-10063396) and a project of Korea Research Institute of Chemical Technology (SI2031-50), Republic of Korea. The chemical library used in this study was kindly provided by Korea Chemical Bank (http://www.chembank.org) of Korea Research Institute of Chemical Technology.

Appendix A. Supplementary data

Supplementary data to this article can be found online at https://doi.org/10.1016/j.neuint.2020.104870.

References

Afrikanova, T., Serruys, A.S., Buenafe, O.E., Clinckers, R., Smolders, I., de Witte, P.A., Crawford, A.D., Esguerra, C.V., 2013. Validation of the zebrafish pentylenetetrazol seizure model: locomotor versus electrographic responses to antiepileptic drugs. PloS One 8, e54166. https://doi.org/10.1371/journal.pone.0054166.

Akaike, N., Moorhouse, A.J., 2003. Techniques: applications of the nerve-bouton preparation in neuropharmacology. Trends Pharmacol. Sci. 24, 44–47.

Armijo, J.A., Shushtarian, M., Valdizan, E.M., Cuadrado, A., de las Cuevas, I., Adín, J., 2005. Ion channels and epilepsy. Curr. Pharmaceut. Des. 11, 1975–2003.

Backus, K.H., Pflimlin, P., Trube, G., 1991. Action of diazepam on the voltage-dependent Na+ current. Comparison with the effects of phenytoin, carbamazepine, lidocaine and flumazenil. Brain Res. 548, 41–49.

Banote, R.K., Koutarapu, S., Chennubhotla, K.S., Chatti, K., Kulkarni, P., 2013. Oral gabapentin suppresses pentylenetetrazole-induced seizure-like behavior and cephalic field potential in adult zebrafish. Epilepsy Behav. 27, 212–219. https://doi.org/10.1016/j.yebeh.2013.01.018.

Baraban, S.C., Dinday, M.T., Hortopan, G.A., 2013. Drug screening in Scn1a zebrafish mutant identifies clemizole as a potential Dravet syndrome treatment. Nat. Commun. 4, 2410. https://doi.org/10.1038/ncomms3410.

Baraban, S.C., Taylor, M.R., Castro, P.A., Baier, H., 2005. Pentylenetetrazole induced changes in zebrafish behavior, neural activity and c-fos expression. Neurosci 131, 759–768.

Begley, D.J., 1996. The blood-brain barrier: principles for targeting peptides and drugs to the central nervous system. J. Pharm. Pharmacol. 48, 136–146.

Brodie, M.J., 2017. Sodium channel blockers in the treatment of epilepsy. CNS Drugs 31, 527–534. https://doi.org/10.1007/s40263-017-0441-0.

Catterall, W.A., 2014. Sodium channels, inherited epilepsy, and antiepileptic drugs. Annu. Rev. Pharmacol. Toxicol. 54, 317–338. https://doi.org/10.1146/annurev-pharmtox-011112-140232.

Cho, S.-J., Byun, D., Nam, T.-S., Choi, S.-Y., Lee, B.-G., Kim, M.-K., Kim, S., 2017. Zebrafish as an animal model in epilepsy studies with multichannel EEG recordings. Sci. Rep. 7, 18112. https://doi.org/10.1038/s41598-017-16993-z.

Cunliffe, V.T., 2016. Building a zebrafish toolkit for investigating the pathobiology of epilepsy and identifying new treatments for epileptic seizures. J. Neurosci. Methods 260, 91–95. https://doi.org/10.1016/j.jneumeth.2015.07.015.

Curia, G., Biagini, G., Perucca, E., Avoli, M., 2009. Lacosamide: a new approach to target voltage-gated sodium currents in epileptic disorders. CNS Drugs 23, 555–568. https://doi.org/10.2165/00023210-200923070-00002.

Dhir, A., 2012. Pentylenetetrazol (PTZ) kindling model of epilepsy. Curr. Protoc. Neurosci. 58, 9–37. https://doi.org/10.1002/0471142301.ns0937s58.

Everett, G.M., Richards, R.K., 1944. Comparative anticonvulsive action of 3,5,5-trimethyloxazolidine-2,4-dione (Tridione), Dilantin and phenobarbital. J. Pharmacol. Exp. Therapeut. 81, 402–407.

Frints, S.G.M., Hennig, F., Colombo, R., Jacquemont, S., Terhal, P., Zimmerman, H.H., Hunt, D., Mendelsohn, B.A., Kordaß, U., Webster, R., Sinnema, M., Abdul-Rahman, O., Suckow, V., Fernández-Jaén, A., van Roozendaal, K., Stevens, S.J.C., Macville, M.V.E., Al-Nasiry, S., van Gassen, K., Utzig, N., Koudijs, S.M., McGregor, L., Maas, S.M., Baralle, D., Dixit, A., Wieacker, P., Lee, M., Lee, A.S., Engle, E.C., Houge, G., Gradek, G.A., Douglas, A.G.L., Longman, C., Joss, S., Velasco, D., Hennekam, R.C., Hirata, H., Kalscheuer, V.M., 2019. Deleterious de novo variants of X-linked ZC4H2 in females cause a variable phenotype with neurogenic arthrogryposis multiplex congenital. Hum. Mutat. 40, 2270–2285. https://doi.org/10.1002/humu.23841.

Gandhi, T., Panigrahi, B.K., Bhatia, M., Anand, S., 2010. Expert model for detection of epileptic activity in EEG signature. Expert Syst. Appl. 37, 3513–3520. https://doi.org/10.1016/j.eswa.2009.10.036.

Goldenberg, M.M., 2010. Overview of drugs used for epilepsy and seizures. P T 35, 392–415.

Grush, J., Noakes, D.L.G., Moccia, R.D., 2004. The efficacy of clove oil as an anesthetic for the zebrafish, Danio rerio (Hamilton). Zebrafish 1, 46–53. https://doi.org/10.1089/154585404774101671.

Jang, I.-S., Nakamura, M., Ito, Y., Akaike, N., 2006. Presynaptic GABAA receptors facilitate spontaneous glutamate release from presynaptic terminals on mechanically dissociated rat CA3 pyramidal neurons. Neuroscience 138, 25–35.

Kim, S.S., Im, S.H., Yang, J.Y., Lee, Y.-R., Kim, G.R., Chae, J.S., Shin, D.-S., Song, J.S., Ahn, S., Lee, B.H., Woo, J.C., Ahn, J.H., Yun, C.S., Kim, P., Kim, H.R., Lee, K.-R., Bae, M.A., 2017. Zebrafish as a screening model for testing the permeability of blood-brain barrier to small molecules. Zebrafish 14, 322–330. https://doi.org/10.1089/zeb.2016.1392.

Lang, D.G., Wang, C.M., Cooper, B.R., 1993. Lamotrigine, phenytoin and carbamazepine interactions on the sodium current present in N4TG1 mouse neuroblastoma cells. J. Pharmacol. Exp. Therapeut. 266, 829–835.

Löscher, W., 2017. Animal models of seizures and epilepsy: past, present and future role for the discovery of antiseizure drugs. Neurochem. Res. 42, 1873–1888. https://doi.org/10.1007/s11064-017-2222-z.

Macdonald, R.L., Kelly, K.M., 1995. Antiepileptic drug mechanisms of action. Epilepsia 36 (Suppl. 2), S2–S12.

May, M., Hwang, K.-S., Miles, J., Williams, C., Niranjan, T., Kahler, S.G., Chiurazzi, P., Steindl, K., Van Der Spek, P.J., Swagemakers, S., Mueller, J., Stefl, S., Alexov, E., Ryu, J.-I., Choi, J.-H., Kim, H.-T., Tarpey, P., Neri, G., Holloway, L., Skinner, C., Stevenson, R.E., Dorsky, R.I., Wang, T., Schwartz, C.E., Kim, C.-H., 2015. ZC4H2, an XLID gene, is required for the generation of a specific subset of CNS interneurons. Hum. Mol. Genet. 24, 4848–4861. https://10.1093/hmg/ddv208.

Murase, K., Ryu, P.D., Randic, M., 1989. Excitatory and inhibitory amino acids and peptide-induced responses in acutely isolated rat spinal dorsal horn neurons. Neurosci. Lett. 103, 56–63.

Nakamura, M., Cho, J.-H., Shin, H., Jang, I.-S., 2019. Effects of cenobamate (YKP3089), a newly developed anti-epileptic drug, on voltage-gated sodium channels in rat hippocampal CA3 neurons. Eur. J. Pharmacol. 855, 175–182. https://doi.org/10.1016/j.ejphar.2019.05.007.

Patsalos, P.N., Berry, D.J., 2012. Pharmacotherapy of the third-generation AEDs: lacosamide, retigabine and eslicarbazepine acetate. Expet Opin. Pharmacother. 13, 699–715. https://doi.org/10.1517/14656566.2012.667803.

Phillips, J.B., Westerfield, M., 2014. Zebrafish models in translational research: tipping the scales toward advancements in human health. Dis. Model. Mech. 7, 739–743. https://doi.org/10.1242/dmm.015545.

Racine, R.J., 1972. Modification of seizure activity by electrical stimulation. II: motor seizure. Electroencephalogr. Clin. Neurophysiol. 32, 281–294.

Randlett, O., Wee, C.L., Naumann, E.A., Nnaemeka, O., Schoppik, D., Fitzgerald, J.E., Portugues, R., Lacoste, A.M., Riegler, C., Engert, F., Schier, A.F., 2015. Whole-brain activity mapping onto a zebrafish brain atlas. Nat. Methods 12, 1039–1046.

Reichel, A., 2006. The role of blood-brain barrier studies in the pharmaceutical industry. Curr. Drug Metabol. 7, 183–203.

Roy, M.L., Narahashi, T., 1992. Differential properties of tetrodotoxin-sensitive and tetrodotoxin-resistant sodium channels in rat dorsal root ganglion neurons. J. Neurosci. 12, 2104–2111.

Scheffer, I.E., Berkovic, S., Capovilla, G., Connolly, M.B., French, J., Guilhoto, L., Hirsch, E., Jain, S., Mathern, G.W., Moshe, S.L., Nordli, D.R., Perucca, E., Tomson, T., Wiebe, S., Zhang, Y.-H., Zuberi, S.M., 2017. ILAE classification of the epilepsies: position paper of the ILAE commission for classification and terminology. Epilepsia 58, 512–521. https://doi.org/10.1111/epi.13709.

Schlossauer, B., Steuer, H., 2002. Comparative anatomy, physiology and in vitro models of the blood-brain and blood-retina barrier. Curr. Med. Chem. 2, 175–186.

Schmidt, D., Sillanpää, M., 2012. Evidence-based review on the natural history of the epilepsies. Curr. Opin. Neurol. 25, 159–163. https://doi.org/10.1097/WCO.0b013e3283507e73.

Sills, G.J., Brodie, M.J., 2001. Update on the mechanisms of action of antiepileptic drugs. Epileptic Disord. 3, 165–172.

Tzallas, A.T., Tsipouras, M.G., Fotiadis, D.I., 2009. Epileptic seizure detection in EEGs using time–frequency analysis. IEEE Trans. Inf. Technol. Biomed. 13, 703–710. https://doi.org/10.1109/TITB.2009.2017939.

Veauthier, J., Haettig, H., Meencke, H.J., 2009. Impact of levetiracetam add-on therapy on different EEG occipital frequencies in epileptic patients. Seizure 18, 392–395. https://doi.org/10.1016/j.seizure.2009.02.001.

Westerfield, M., 2000. The Zebrafish Book: A Guide for the Laboratory Use of Zebrafish (Danio Rerio), fourth ed. University of Oregon press, Eurgene.

Wilcox, K.S., Dixon-Salazar, T., Sills, G.J., Ben-Menachem, E., White, H.S., Porter, R.J., Dichter, M.A., Moshé, S.L., Noebels, J.L., Privitera, M.D., Rogawski, M.A., 2013. Issues related to development of new antiseizure treatments. Epilepsia 54 (Suppl. 4), 23–34. https://doi.org/10.1111/epi.12296.

World Health Organization, 2019. Epilepsy. https://www.who.int/news-room/fact-sheets/detail/epilepsy. (Accessed 20 April 2020).